HURRICANE IMAGING RADIOMETER WIND SPEED AND RAIN RATE RETRIEVAL: PART-2. ANALYSIS OF RETRIEVAL ACCURACY

Ruba A. Amarin[1], Linwood Jones[1], James Johnson[1], Chris Ruf[2], Tim Miller[3] and Shuyi Chen[4]

[1] Central Florida Remote Sensing Laboratory
University of Central Florida, Orlando, Florida 32816, U.S.A
** ramarin@mail.ucf.edu*
[2] Space Physics Research Laboratory, University of Michigan, Ann Arbor, Michigan
[3] NASA Marshall Space Flight Center, Huntsville, Alabama
[4] University of Miami, Miami, Florida

ABSTRACT

This paper describes the end-to-end simulation of the new HIRAD, which will provide improved hurricane surveillance. This paper (part-2 of 2) evaluates the HIRAD instrument performance in retrieving hurricane-force wind speeds in the presence of intense rain. Examples of retrieved hurricane wind speed and rain rate images are presented, and comparisons of the retrieved parameters with the MM5 numerical hurricane model data are made. Statistical results are presented over a broad range of wind and rain conditions over the full measurement swath.

Index Terms— HIRAD, imaging, hurricanes, retrievals, wind speed, rain rate

1. INTRODUCTION

The Hurricane Imaging Radiometer, HIRAD, is a next generation Stepped Frequency Microwave Radiometer, SFMR, [1] for improved airborne surveillance of ocean surface winds and rain in hurricanes. HIRAD is a multi-frequency microwave radiometer at C-band that uses synthetic aperture thinned array radiometry technology to create a 1-D microwave imager that synthesizes brightness temperature, T_b, images cross track and provides real aperture imaging along track [2]. This technology is currently under development at the NASA Marshall Space Flight Center in a collaborative effort with NOAA Hurricane Research Division, the Central Florida Remote Sensing Laboratory (CFRSL) at the University of Central Florida (UCF) and the University of Michigan.

This paper deals with the remote sensing of wind speed and rain rate in hurricanes, which directly supports the HIRAD instrument development. Through the use of realistic simulations of hurricane surveillance flights over ocean, we are able to predict the wind speed measurement performance of a conceptual pushbroom wide-band radiometer system that has strong similarities with HIRAD. The goal of this research is to use this simulation to characterize the HIRAD hurricane surface wind speed measurement accuracy as a function of wind speed, rain rate and cross-swath location (earth incidence angle, EIA). We use proven methods of microwave radiometer measurement modeling in a Monte Carlo simulation to predict wind speed retrieval errors parametrically with instrument characteristics, and the results of the simulation are directly applicable to the HIRAD performance.

2. HIRAD EQUIVALENT PUSHBROOM RADIOMETER SYSTEM

In this paper, results are presented for a simulated real aperture pushbroom radiometer equivalent of HIRAD, which is shown in Fig. 1. In the simplest terms, the equivalent system replaces the HIRAD synthetic thinned array imaging with 41 individual antenna beams (with boresight spaced on 3^o centers $\pm 60^o$). These beams are contiguous at nadir and they overlap at the edges of the swath.

The pushbroom antenna beams were implemented as 4 different antenna designs (one per frequency) that are scanning phased arrays that produce similar patterns to the synthesized beams for HIRAD. Thus, the pushbroom patterns are equivalent in terms of the C-band operating frequencies, approximate antenna pattern spatial resolutions, cross-track boresight pointing angles (every 3^o) and polarization. The HIRAD antenna is designed to measure the horizontally polarized brightness temperature emission from the surface over $\pm 60^o$ in the cross-track direction.

Figure 1 Equivalent real-aperture radiometer system with 41 beams cross-track.

3. HURRICANE FORWARD RADIATIVE TRANSFER MODEL

As part of the HIRAD development, the CFRSL radiative transfer model, RTM, was tuned for hurricane environment. The selected approach was to use the SFMR rain algorithm, which is derived from the work of Jorgensen and Willis [5] and Olsen et al. [6], and to develop an improved microwave radiometric ocean surface emissivity model (part-1 of 2) [7].

3.1. Atmosphere Forward Model

The RTM [8], has 39 atmospheric layers of 20 km total thickness, which are used to compute the water vapor, cloud liquid water and oxygen absorption coefficients. For the HIRAD frequencies, only water vapor and cloud liquid absorption in hurricanes are significant.

The MM5 hurricane "nature run" simulations were from a state-of-art numerical model described by Chen et al. (2007) [9]. A model run for Hurricane Frances (2004) provides realistic 3D environmental parameters (rain, water vapor, clouds and surface winds) from which simulated HIRAD T_b's are derived for typical aircraft "Fig-4" flight tracks. The MM5 model uses a system of nested grids with the innermost one having a horizontal grid spacing of 0.015 degrees (~1.6 km resolution) in longitude and latitude.

In the forward radiative transfer model, we use 3D environmental components produced by the MM5 nature run. Each simulated HIRAD measurement (cross-track pixel) will have a unique surface wind speed and atmospheric profile, which uses a mesh grid criterion by dividing the atmosphere into 39 layers and the ground into 1.67 km pixels (corresponding to the MM5 resolution) as shown in Fig. 2. This procedure approximates the actual HIRAD T_b measurement whereby the upwelling and downwelling T_b components to be calculated along a different slant path. The pushbroom antenna boresight geometry calculations are performed based on the HIRAD antenna sampling for the cross-track scans.

3.2. Antenna Brightness Temperature

The simulation uses a real aperture phased array antenna to produce multiple antenna beams in a pushbroom configuration for the wide-swath surface sampling, which is approximately equivalent to the HIRAD brightness temperature image synthesis. The HIRAD measurement is horizontal (H-pol) but the cross-polarization (V-pol) must also be included. Therefore, both the H-Pol and V-Pol scene apparent T_b are computed from the forward model and are convolved with the co-polarized (Co-Pol) and cross-polarized (X-Pol) antenna patterns respectively. The resulted convolved H-Pol and V-Pol temperatures are given by [10],

$$T_{bH\_conv} = \frac{\int_0^{2\pi}\int_{-\theta}^{\theta} T_{ap\,h}(\theta,\Phi)\times F_{Co-Pol}(\theta,\Phi)\times sin\theta d\,\theta d\Phi}{\int_0^{2\pi}\int_{-\theta}^{\theta} F_{Co-Pol}(\theta,\Phi)\times sin\theta d\,\theta d\Phi} \quad (3)$$

$$T_{bV\_conv} = \frac{\int_0^{2\pi}\int_{-\theta}^{\theta} T_{apv}(\theta,\Phi)\times F_{X-Pol}(\theta,\Phi)\times sin\theta d\,\theta d\Phi}{\int_0^{2\pi}\int_{-\theta}^{\theta} F_{X-Pol}(\theta,\Phi)\times sin\theta d\,\theta d\Phi} \quad (4)$$

In (3), the horizontally convolved T_b is integrated over $\pm\theta_1 = \pm 30^o$ that results in ~ 100% beam efficiency for the Co-Pol antenna pattern, whereas in the vertically convolved T_b given by (4), the θ limits change by beam position to insure > 90% beam efficiency.

The final convolved brightness temperature, T_A, is a superposition of T_{bH_conv} and T_{bV_conv} according to,

$$T_A = (1-\gamma)T_{bH_{conv}} + \gamma T_{bV\_conv} \quad (5)$$

where γ is the ratio of the X-Pol brightness temperature to the total and is approximated by,

$$\gamma = \frac{\int_{FirstNulls} XPol}{\int_{FirstNulls} XPol + \int_{FirstNulls} CoPol} \quad (6)$$

γ changes as a function of incidence angle (beam position) for each frequency and increases with angles; for the nadir beam (Fig. 3(a)), nearly all the brightness is from Co-Pol making γ approximately equal to zero. On the other hand, for the beam position at 60^o (Fig. 3(b)), where both patterns have the same power gain, results in approximately half of the measured brightness coming from X-Pol and half from the Co-Pol, making $\gamma \sim 0.5$.

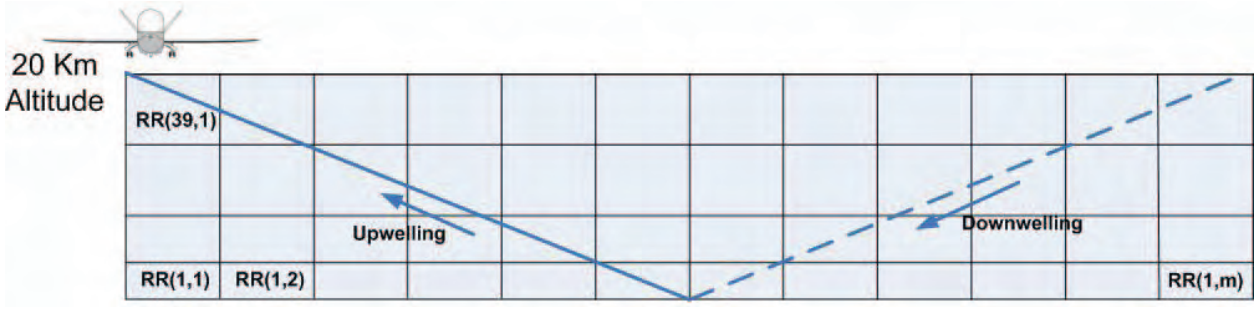

Figure 2 Forward model simulation.

4. GEOPHYSICAL RETRIEVAL ALGORITHM

A retrieval algorithm known as the Hurricane Imaging Retrieval Algorithm was developed for rain rate and wind speed retrievals in hurricanes. It is composed of a forward radiative transfer model and an inversion algorithm.

4.1. Atmospheric Treatment

The retrieval algorithm forward model is different than the forward model used in the simulation. First, the treatment of the atmosphere used in the retrieval is considered to be homogeneous and constant along the line of sight at each beam position, while in the simulated forward model, the atmosphere is varying in 3D as described earlier. Water vapor and cloud liquid water annuli of 5 km thicknesses were constructed from the MM5 data. Each annulus was assigned the mean value of the data that are circumscribed by it which results in water vapor and cloud liquid water profiles. The sum of these absorption coefficients along with an additional absorption coefficient due to rain is used in the computation of the modeled brightness temperature (T_{mod}) at each of the four C-band frequencies. These T_b's are placed into a three dimensional matrix for each frequency with wind speed, rain rate and angles as variables.

Another major difference between the RTM's is in the treatment of rain. In the retrieval, the rain is assumed to be uniform along the slant path from the constant freezing level of 5 km to the surface, while in the simulated forward model the freezing level varies as does the 3D distribution of rain. As noted in Fig. 2, for the retrieval, the upwelling and the reflected downwelling T_b from rain assume the same uniform rain rate.

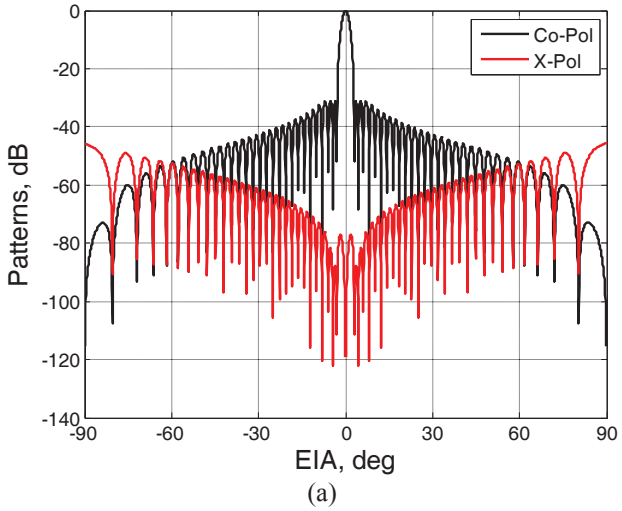

(a)

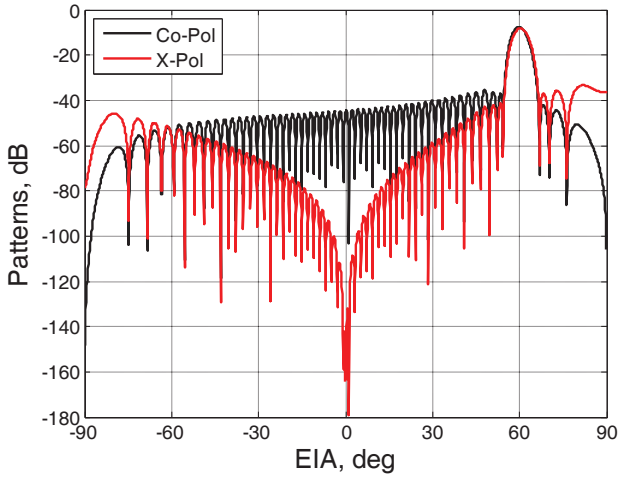

(b)

Figure 3 Co-Pol and X-Pol patterns at 6.6 GHz frequency for (a) 0^o and (b) 60^o scan beams.

4.2. Antenna Pattern Correction

In order to correct for the antenna pattern convolution effect in the retrieval algorithm, the V-Pol effect was removed from the total antenna brightness temperature (T_A) computation according to,

$$T_{bH\_conv} = \frac{T_A - \gamma \times T_{bV\_conv}}{(1-\gamma)} \quad (7)$$

The V-Pol convolved temperatures, T_{bV_conv}, in (7) are estimated based on the best linear fit relationships with the convolved brightness temperature, T_A.

After solving for T_{bH_conv}, the T_b due to the antenna pattern was corrected for as shown in (8),

$$T_{Corr} = \frac{1}{\eta_{ML}} [T_{bHconv} - \eta_U \times T_U - \eta_B \times T_B] \quad (8)$$

where T_U and T_B are the brightness temperatures that correspond to the "above the boresight" and "below the boresight" portions of the pattern. These T_b's are computed as part of the simulated forward model based on the best linear fit relationships with T_A.
η_{ML}, η_U, and η_B are the correspondent beam efficiencies of the main lobe, above and below the boresight respectively.

4.3. Retrieval Algorithm

After correcting for the antenna pattern effect, random errors are included in the simulation, which represent the NEDT and the ΔG/G instrument noises. In the simulation, these errors are additive zero mean Gaussian random distributions with standard deviations that vary parametrically from 1 to 8 Kelvin (even though the expected HIRAD instrument noise does exceed a couple of Kelvin).

The modeled brightness temperature matrix, T_{mod}, is compared to the corrected brightness temperature with random errors added, (T_{corr} + *Noise*), at each of the four frequencies. Each element in the difference matrices is squared and the algorithm searches for the minimum of the summed squared difference surface, over all frequencies. This process is repeated 50 times in a Monte-Carlo simulation for each beam position and scan to collect RMSE statistics.

5. RESULTS

Comprehensive simulations for assessing HIRAD performance were conducted. The wind (see Fig. 4(a)) and rain fields from the hurricane Frances modeled data were used. The most common flight pattern used is the "Fig-4" where the aircraft flies two passes, normal to each other, through the center of the eye. Each flight leg is approximately 350 km long as illustrated in Fig. 4(b, c). The maximum wind speed and rain rate in these two passes are ~ 60 m/s and ~ 120 mm/hr respectively as resented by the colorbar. These two passes show that HIRAD would cover the eyewall region in most hurricanes with a single standard "Fig-4" pattern.

Results include computing the retrieved wind speed errors at each added random instrument noise level, and the statistics are summarized in Table 1. As noted from the table, the standard deviation values increase with increasing the instrument noise as expected. At zero std instrument noise, the resultant errors are mainly due to the antenna pattern effect specially at larger angles and the different atmospheric treatment in both the forward model and the retrievals.

TABLE I
RETRIEVED WIND SPEED ERROR STATISTICS

Random Instrument Error std (Kelvin)	0	1	2	4	8
Mean	1.945	1.903	1.824	1.494	0.525
Std	1.587	1.835	2.404	4.030	7.792

Retrievals for multiple cross-track scans, forming one complete flight pattern leg, were simulated and compared to the nature run "surface truth" wind field, and the rms differences (for the 1 Kelvin random error case) are plotted for both orthogonal legs in Fig. 5. The colorbar represents the rms wind speed error values, which are higher at larger incidence angles. Higher wind speed errors occur at the edges of the swath where path lengths are greatest and rain is the most intense in that eye wall region.

5. SUMMARY & CONCLUSION

HIRAD simulation for wide swath microwave brightness temperature observations of a hurricane and retrieval algorithms for surface wind speed and rain rate have been developed. Nature run using the MM5 numerical model for wind and rain fields for hurricane Frances, 2004 were used in estimating HIRAD wind speed retrieval errors. Retrieval algorithm was based on the HIRAD geometry, and an equivalent HIRAD antenna design. Realistic aircraft surveillance flight patterns through Frances were simulated, including instrument errors. The retrieved wind field compares well to the surface truth over most of the swath, but antenna pattern effects along with differences in the atmosphere treatment caused some large wind speed errors near ± 60^o in the presence of intense rain.

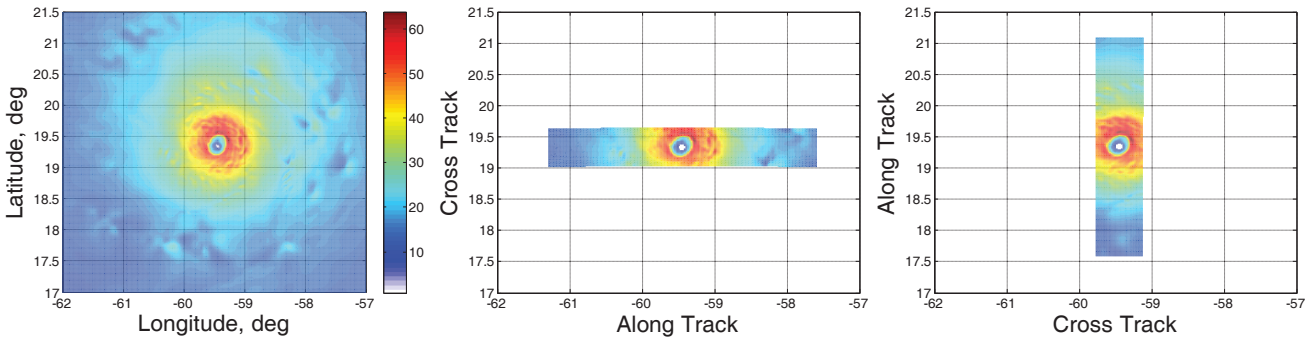

Figure 4 Surface truth wind field (a) image, (b) leg 1 and (c) leg 2.

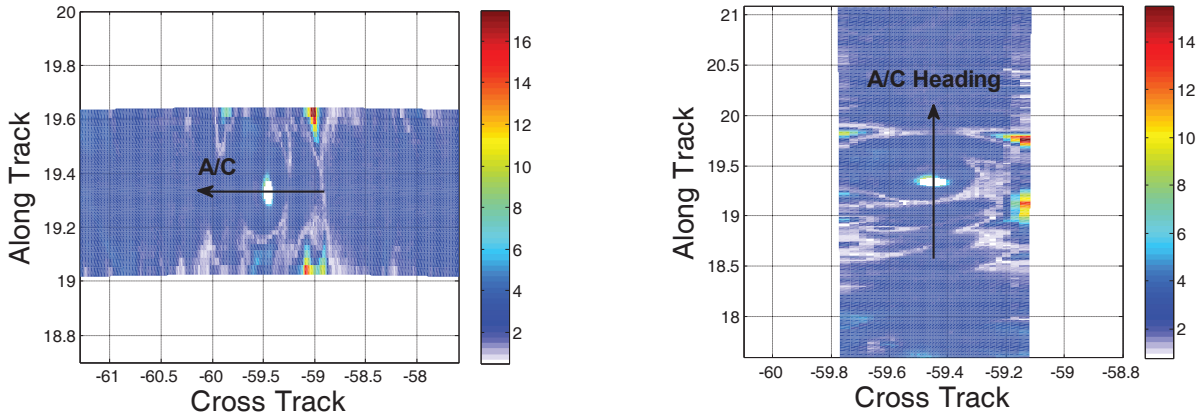

Figure 5 RMS retrieved wind speed errors for (a) leg 1 and (b) leg 2.

6. REFERENCES

[1] E. W. Uhlhorn, P. G. Black, J. L. Franklin, M. Goodberlet, J. Carswell, A. S. Goldstein "Hurricane Surface Wind Measurements from an Operational Stepped Frequency Microwave Radiometer," *American Meteorological Society*, 2007.

[2] A. B. Tanner and C. T. Swift, "Calibration of a Synthetic Aperture Radiometer," *IEEE Trans. Geosci. Remote Sensing*, vol. 31, pp. 257-267, Jan. 1993.

[3] C. Ruf, B. Lim, R. Amarin, J. Johnson, L. Jones, M. C. Bailey, M. James, R. Hood, K. Stephens, V. Rohwedder, "The Hurricane Imaging Radiometer – An Octave Bandwidth Synthetic Thinned Array Radiometer", *Proc. IGARSS 2007*, Barcelona, July 2007.

[4] Boon H Lim, Ruba Amarin, Salem El-Nimri, James Johnson, Linwood Jones and Christopher S Ruf, "Restrictions on the Field of View for an Undersampled 1-D Synthetic Thinned Aperture Radiometry", *Proc. IGARSS 2007*, Barcelona, July 2007.

[5] D. P. Jorgensen and P. T. Willis, "A Z-R Relationship for Hurricanes," *Journal of Applied Meteorology*, vol. 21, pp. 356-366, 1982.

[6] R. L. Olsen, D. V. Rogers, and D. B. Hodge, "The aR^b Relation in the Calculation of Rain Attenuation," *IEEE Trans. Antennas Propagat.*, vol. 26, pp. 318-329, 1978.

[7] Salem Fawwaz El-Nimri, W. Linwood Jones, Eric Uhlhorn, Christopher Ruf , James Johnson, and Peter Black, "An Improved C-band Ocean Surface Emissivity Model at Hurricane-force Wind Speeds over a Wide Range of Earth Incidence Angles," *IEEE Geoscience and Remote Sensing Letters*, 2009.

[8] Linag Hong, "Inter-Satellite Microwave radiometer Calibration", Ph.D. Dissertation, University of Central Florida, School of EECS, 2008.

[9] Chen, S. S., J. F. Price, W. Zhao, M. A. Donelan, E. J. Walsh, "The CBLAST-Hurricane Program and the Next-Generation Fully Coupled Atmosphere-Wave-Ocean Models for Hurricane Research and Prediction," *Bull. Amer. Meteor. Soc.*, 88(3), 311-317, 2007.

[10] F. T. Ulaby, R. K. M. Moore, and A. K. Fung, "Microwave Remote Sensing, Active and Passive", vol. 1. Chapter 4, Section 4.5, pp. 203-208, Norwood, MA: Artech House Inc, 1981.